

Low Temperature Thermal Properties of Nanodiamond Ceramics

Daria Szewczyk ^{1,2,*}  and Miguel A. Ramos ^{2,3}

¹ Department of Low Temperature and Superconductivity, Institute of Low Temperature and Structure Research PAS, Okólna 2, 50-422 Wrocław, Poland

² Departamento de Física de la Materia Condensada & Instituto “Nicolás Cabrera”, Universidad Autónoma de Madrid, Francisco Tomás y Valiente 7, 28049 Madrid, Spain

³ Centro de Microanálisis de Materiales (CMAM), Universidad Autónoma de Madrid, Faraday 3, 28049 Madrid, Spain

* Correspondence: d.szewczyk@intibs.pl

Abstract: The temperature dependence of thermal conductivity and specific heat for detonated nanodiamond ceramics is investigated on specially designed experimental setups, implementing the uniaxial stationary heat flow method and the thermal relaxation method, respectively. Additionally, complementary studies with a commercial setup (Physical Property Measurement System from Quantum Design operating either in Thermal Transport or Heat Capacity Option) were performed. Two types of samples are under consideration. Both ceramics were sintered at high pressures (6–7 GPa) for 11–25 s but at different sintering temperatures, namely 1000 °C and 1600 °C. The effect of changing the sintering conditions on thermal transport is examined. In thermal conductivity $\kappa(T)$, it provides an improvement up to a factor of 3 of heat flow at room temperature. The temperature dependence of $\kappa(T)$ exhibits a typical polycrystalline character due to hindered thermal transport stemming from the microstructure of ceramic material but with values around 1–2 W/mK. At the lowest temperatures, the thermal conductivity is very low and increases only slightly faster than linear with temperature, proving the significant contribution of the scattering due to multiple grain boundaries. The specific heat data did not show a substantial difference between detonated nanodiamond ceramics obtained at different temperatures unlike for $\kappa(T)$ results. For both samples, an unexpected upturn at the lowest temperatures is observed—most likely reminiscent of a low-T Schottky anomaly. A linear contribution to the specific heat is also present, with a value one order of magnitude higher than in canonical glasses. The determined Debye temperature is 482 (± 6) K. The results are supported by phonon mean free path calculations.

Keywords: nanodiamond ceramic; thermal conductivity; specific heat; low temperature phenomena; sintering



Citation: Szewczyk, D.; Ramos, M.A. Low Temperature Thermal Properties of Nanodiamond Ceramics. *Crystals* **2022**, *12*, 1774. <https://doi.org/10.3390/cryst12121774>

Academic Editor: Jorge Souto

Received: 31 October 2022

Accepted: 3 December 2022

Published: 7 December 2022

Publisher's Note: MDPI stays neutral with regard to jurisdictional claims in published maps and institutional affiliations.



Copyright: © 2022 by the authors. Licensee MDPI, Basel, Switzerland. This article is an open access article distributed under the terms and conditions of the Creative Commons Attribution (CC BY) license (<https://creativecommons.org/licenses/by/4.0/>).

1. Introduction

Detonated nanodiamonds have become one of the most interesting and intensely exploited carbon materials in the past few decades [1,2]. This is especially true after establishing their sintering procedure, which started back in the 1980s [3,4] and which is now fully implemented in the industry with widely used technology. The high demand for the use of nanodiamond materials has been derived from their exceptional properties like mechanical performance, electrical, optical, thermal, even biocompatible ones [5,6]. Most importantly it is their vast possible applications that make them so desirable [7–12].

While the common approach covers the structural, electrical, and strength tests, or materials functionalization, an increase in the importance of thermal properties was also observed. Next to the fundamental science, an equally critical issue of heat removal, enhanced by practical needs, awaited its progress mostly due to the growth in the electronic industry requiring a good determination of the dissipated thermal energy. [13,14] Another noticeable effect needing detailed consideration is the change in thermal behavior with

the lowering of the size to the nanometer scale. Nanomaterials do not transfer heat in the same manner as their bulk crystalline counterparts [15,16]. It is mostly inherited from the increased phonon-boundary scattering or changes in the phonon dispersion [17,18]. Nanoscale thermal transport requires also a completely different approach when it comes to simulation [19].

Thermal transport mechanisms in carbon materials are of different natures depending on the scale (macro/micro/nano) and type. Due to the vast spread of data in the literature, the focus will be limited only to the nanodiamond ones. Investigations on the thermal conductivity of nanodiamond and microdiamond samples and their composites were so far carried out by different groups by using both stationary and transient methods, e.g., [20–22]. In all the mentioned papers the focus was on the determination of the final thermal conductivity value at room temperature depending on the origin or different sintering conditions of detonated nanodiamond material towards desired high values of the parameter. On the other side, heat capacity studies were substantially less common and performed only in a limited temperature range [23].

The materials chosen for studies are two types of nanodiamond ceramic samples obtained by sintering at high pressures in a toroidal chamber of detonated nanodiamond powders at different temperatures. Besides testing the assumption that higher sintering temperature provides better thermal transport in samples, we mostly focus on some unexplored fields, namely the possible phenomena associated with the temperature dependence of thermal conductivity coefficient and specific heat, particularly in the low-temperature region [24,25].

2. Materials and Methods

2.1. Samples

The sintering of polycrystalline detonated nanodiamond ceramics was carried out in a high-pressure toroid-type chamber of 0.26 cm³ in volume, using a press with the axial force of 5 MN. AC current at 50 Hz in the electric power stabilization regime heated the initial blend in a graphite cylinder. The as-received sintered samples were cylinders of approx. ~3 mm in diameter and ~4 mm high. The chamber pressure was maintained in the range of ~6.0 to 6.5 GPa, the sintering temperature was ~1000 °C or 1600 °C for particular samples, respectively and the annealing time varied from 11 to 25 s. Under these conditions, the structure of diamond is preserved, as confirmed by XRD (see Supporting Information Figure S1). The details of the detonation nanodiamond technology can be found in [2,26,27]. The sample sintered at 1600 °C will be named **dnd_crmc1** hereafter, and the one sintered at 1000 °C as **dnd_crmc2**.

2.2. Thermal Conductivity

Thermal conductivity experiments were carried out in a specially designed heat bath cryostat at the Department of Low Temperature and Superconductivity, Institute of Low Temperature and Structure Research, Polish Academy of Sciences, (ILT&SR PAS), in Wrocław, Poland, utilizing the stationary uniaxial heat flow method. The chosen samples were of cylindrical shape with an average diameter of $\phi = 2.75$ mm and height of 3.55 mm (**dnd_crmc1**) and 3.89 mm (**dnd_crmc2**). On the top of each sample, a resistive heater was attached with special glue in order to induce heat flux along the sample. On the other end, the sample was anchored to the so-called cold finger serving as a heat bath reservoir. The temperature gradient was measured with two constantan–manganin thermocouples spaced between each other at 1.1 mm (**dnd_crmc1**) and 1.24 mm (**dnd_crmc2**), respectively. The details of the operation of the experimental device can be found in [28]. Additional experiments were performed utilizing the Physical Property Measurement Systems (PPMS) from Quantum Design, operating in the Thermal Transport Option with the stationary method chosen for measurements. A picture of the sample mounted on the TTO sample puck is shown in Figure 1. The methodology is analogous to the one implemented in the ILT&SR PAS device. Interested readers are referred to the operator's manual [29]

or [30]. The advantage of performing additional studies on the commercial setup is the extended temperature range down to 1.8 K, and the reason to continue performing the experiments on the specially constructed device is its higher accuracy, especially at higher temperatures, where the multiple shielding provides excellent isolation, and all the parasitic effects are eliminated.

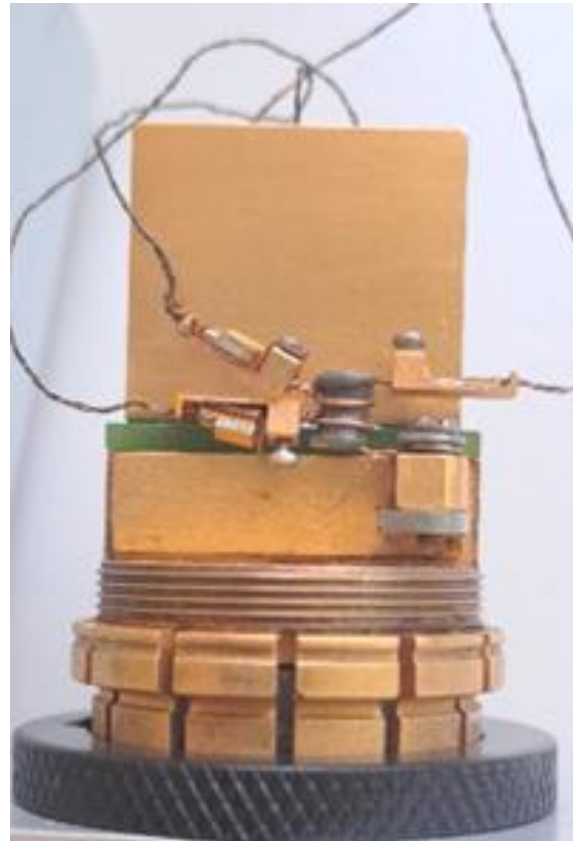


Figure 1. Detonated nanodiamond ceramic sample mounted on the TTO sample puck of PPMS in a 4-wire contact configuration.

2.3. Heat Capacity

As in the case of thermal conductivity, heat capacity measurements were also performed in two complementary devices. The calorimetric system at the Low Temperature Laboratory of the Universidad Autónoma de Madrid (UAM) essentially uses two kinds of methods which, according to the investigated temperature range, can be selected: namely, a particular quasi-adiabatic continuous method in a wide temperature range, and the thermal relaxation method typically below 30 K, in turn being able to choose between the standard relaxation method and a non-standard, faster relaxation one [31,32]. The standard relaxation method requires first the achievement of the steady-state equilibrium between cooling and heating power, and second the recording of the temperature relaxation after switching off the heating power. A faster relaxation method skips waiting for the equilibrium condition and utilizes the heating curve of the recorded data. As in all calorimetric heat-capacity experiments, a separate measurement of the empty cell is performed and subtracted from the final results to assess the net specific heat. The commercial device, again the Physical Property Measurement System from Quantum Design, but here operating in the Heat Capacity Option, at the disposal of the ILT&SR PAS, utilizes the standard relaxation method [33]. The main advantages of the versatile calorimetric setup at UAM, in relation to the commercial device, are the possibility to change the measuring method in a particular temperature range and to cool the sample cell with relatively high cooling rates (in the commercial one limited to an effective pace of about 10 K/min). Another signifi-

cant advance that distinguishes the UAM system is the possibility to also measure liquid materials by means of a specially designed calorimetric sample cell. Further information on the setup can be found in [31,32]. The details of the heat capacity measurements in the commercial device are provided in [34]. The illustration of particular samples mounted into the calorimeters is presented in Figure 2. One should notice that the UAM setup contains much more sample space—the sapphire disk, on which the sample is mounted, is around $\phi = 25.4$ mm in diameter and the sample can be placed as a whole, while the sample table of the commercial PPMS is a square approximately 3×3 mm and a small sample piece needs to be cut out. The weights of the particular samples used for the measurements are summarized in Table 1.

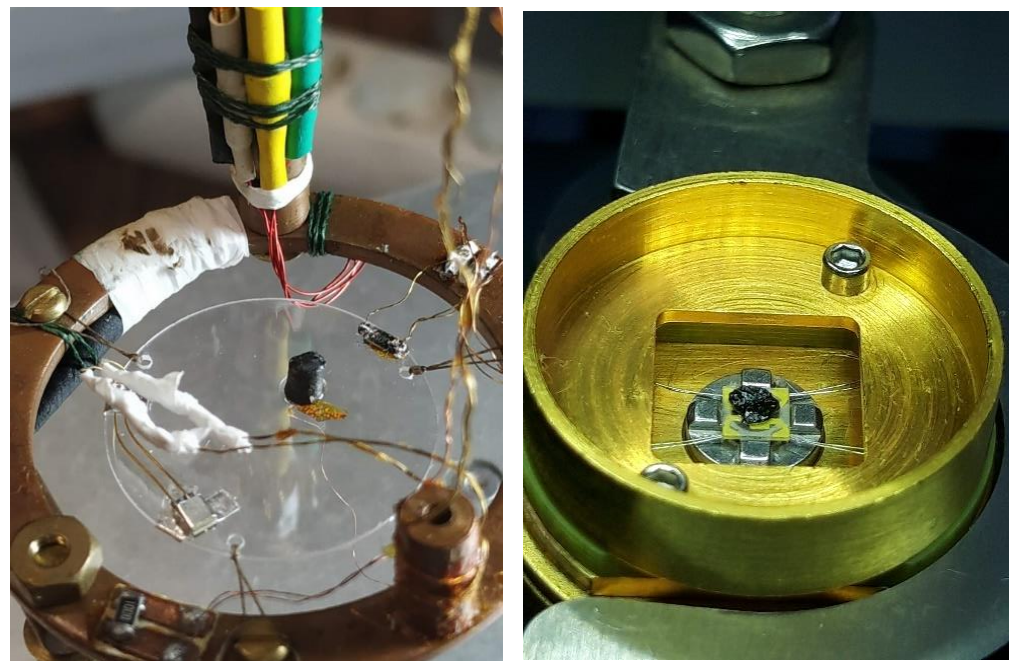


Figure 2. Detonated nanodiamond ceramic samples in different experimental setups for heat capacity measurements. (Left): dedicated calorimetric cell of the cryostat at UAM; (Right): sample puck of commercial PPMS at ILT&SR PAS.

Table 1. Sample masses of particular detonated nanodiamond samples used in different experimental setups.

Sample	Mass UAM [mg]	Mass PPMS [mg]
dnd_crnc1	53.08	5.35
dnd_crnc2	57.25	2.87

3. Results and Discussion

3.1. Thermal Conductivity

Thermal conductivity measurements were carried out in a temperature range of 1.8 K–300 K (in PPMS setup) and 4.2 K–300 K (in ILT&SR design setup). The results are presented in Figure 3 (red symbols—**dnd_crnc1** sample sintered at 1600 °C; blue symbols—**dnd_crnc2** sample sintered at 1000 °C; filled stars symbols correspond to experiments performed on the specially designed cryostat; empty symbols refer to PPMS measurements).

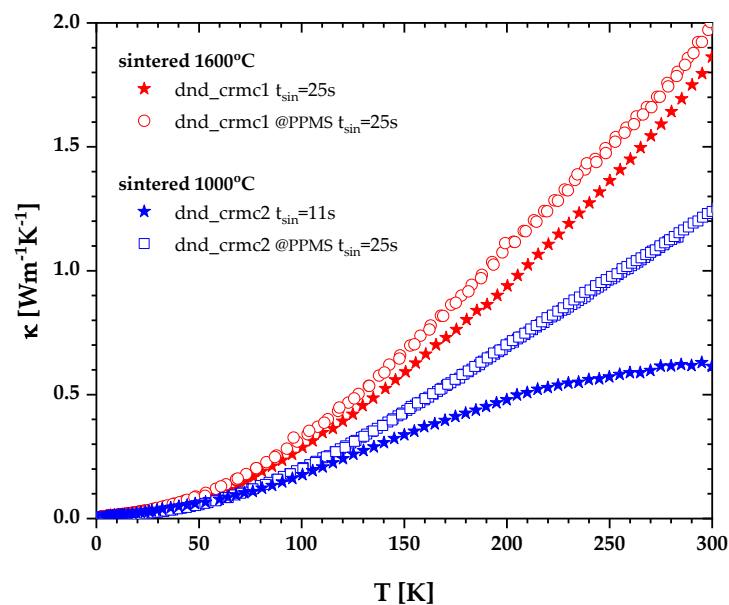


Figure 3. Thermal conductivity as a function of temperature for detonated nanodiamond ceramic samples sintered at different temperatures and measured in two different setups.

The thermal conductivity of the detonated nanodiamond ceramics decreases monotonically upon lowering the temperature in the whole investigated temperature range. For the samples sintered at 1600 °C (red symbols) the agreement between the results obtained in different setups is satisfactory. What can be seen in the graph, especially at high temperatures, is the additional radiative contribution to the total thermal conductivity. This issue of the PPMS system was thoroughly described before in the literature [35]. Above 150 K the relative difference is 0.13 W/mK on average, which then drops evenly down to approximately 0.03 W/mK at 50 K. At the lowest investigated temperatures, thermal conductivity measured in both experimental setups overlaps within the experimental error. In the second case of detonated nanodiamond ceramic sintered at 1000 °C the situation is more complex from the start. There is no straightforward agreement between the results obtained in the two cases. The reason behind this might be the fact that the experiments were performed on two different samples (unlike in the previous case), both sintered at 1000 °C, but with different sintering times, which could also have influenced the resulting sample properties, as shown in Figure 3. Increasing the sintering time from 11 to 25 s at 1000 °C clearly improves the thermal conductivity by a factor of 2. While keeping the sintering time constant, at 25 s, and changing the temperature from 1000 °C to 1600 °C, the thermal conductivity increases by 1.5 at room temperature. The studies of the sintering temperature's powerful influence on the resulting thermal conductivity were presented in [20], c.f. Table 1 of [36]. In our case, an additional reason for this perceptible difference in absolute values of thermal conductivity might be the changing contribution of the phonon processes responsible for the thermal transport mechanisms. As the samples are polycrystalline ceramics, what is reflected, among others, by the observed temperature dependence of the $\kappa(T)$, the prevailing factor strongly affecting the heat flow in the bulk material is the multiple grain boundaries. The particularly sensitive region, where the phonon scattering processes on grain boundaries have their most relevant contribution to hindering the thermal transport, is the low temperature. For this reason, the range of interest is presented in a close-up in Figure 4.

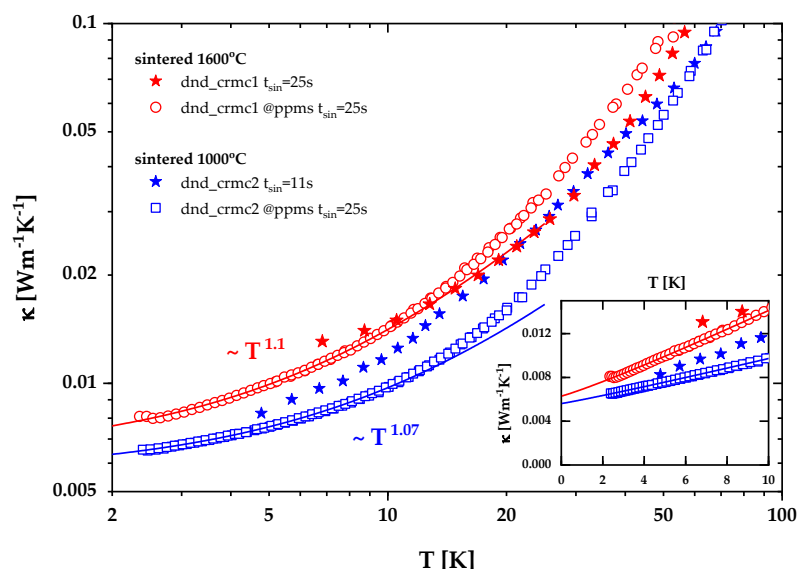


Figure 4. Low temperature thermal conductivity of differently prepared detonated nanodiamond ceramics. *Insert:* $\kappa(T)$ data in a linear scale up to 10 K.

The phenomena observed in the investigated materials are of complex nature. They comprise a nanoscale behavior of a different type stemming from the building nanomaterial of the ceramics, but also a macroscale contribution due to the ceramic grainy structure itself. The alternation of the dominant heat transfer mechanism for the case of diamond-based materials was stressed in [37]. At the lowest temperatures, the investigated ceramics exhibit more than three orders of magnitude lower values of thermal conductivity coefficient than in the case of a bulk diamond [38] nearing the lower limit of the thermal conductivity of disordered crystals proposed by Cahill et al. [39]. The temperature dependence of the detonated nanodiamond resembles in shape the $\kappa(T)$ results of diamond films [40] but again with substantially lower values, yet corresponds to results of previous nanodiamond composite samples [21,22,41]. In Figure 4, up to 10 K, the thermal conductivity coefficient as a function of temperature was approximated with $\kappa \sim T^{1.07}$ (sample sintered at 1000 °C) and $\kappa \sim T^{1.1}$ (sample sintered at 1600 °C), shown additionally as an insert in Figure 4. Such a low value of the exponent is mostly caused by the strong hindrance of the heat flow due to grain boundaries.

3.2. Heat Capacity

The heat capacity investigations, as in the case of thermal conductivity coefficient, were performed on two complementary setups. The PPMS measurements were carried out in the temperature range 1.8 K–300 K. The results are presented in Figure 5 in a log–log scale (red open circles describe the data from sample sintered at 1600 °C; blue open squares the ones from sample sintered at 1000 °C). Detailed studies in the range 1.8 K–30 K were additionally carried out on the specially designed low temperature calorimetric system at the UAM. The low temperature analysis covering the experimental data from both setups is presented in Figures 6 and 7.

Unlike thermal conductivity data, the specific heat in the two detonated nanodiamond ceramics is found to be almost identical at the investigated temperatures. The temperature relation nicely corresponds to the results of Vasiliev et al. [23]. Above 50 K the temperature dependence can be roughly approximated with $C_p \sim T^{1.97}$. The room temperature values are 658 mJ/g K and 710 mJ/g K for the **dnd_crnc1** (sintered at 1600 °C) and **dnd_crnc2** (sintered at 1000 °C), respectively, which is a bit higher than the specific heat of nanodiamond arrays 630 mJ/g K by Su et al. in [19], or diamond/carbon composites with different ratios of sp²/sp³-bonded carbon which yielded from 510 mJ/g K up to 610 mJ/g K c. f. Table 1 in [21].

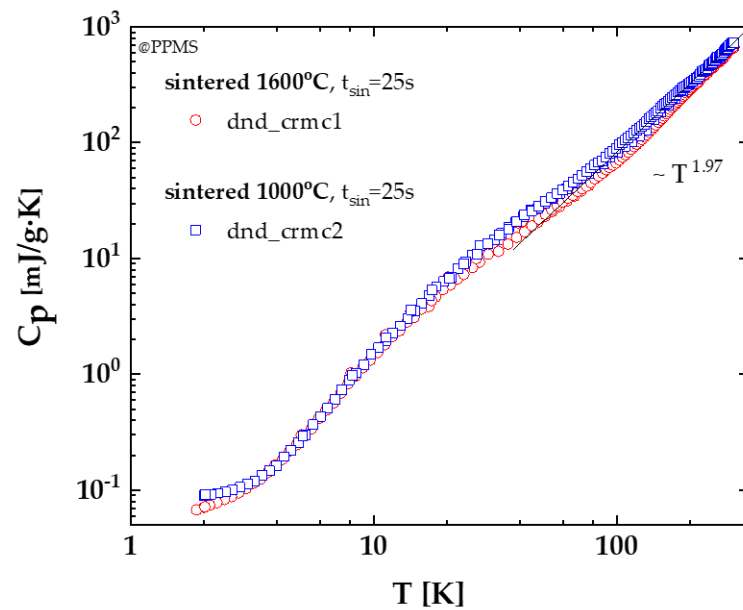


Figure 5. Specific heat as a function of temperature of detonated nanodiamond ceramics sintered at different temperatures measured with PPMS.

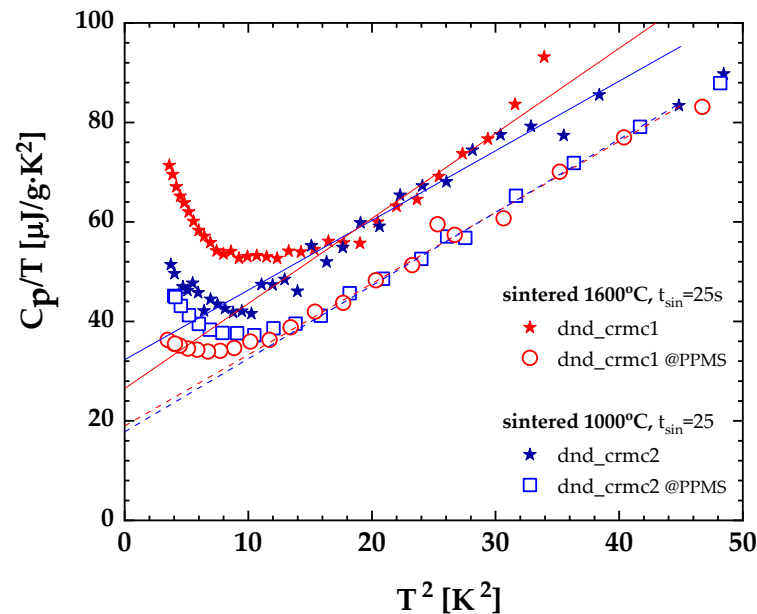


Figure 6. Low temperature specific heat in C_p/T representation as a function of square temperature for differently sintered detonated nanodiamond ceramics, measured at two complementary setups.

For the lower temperatures, additional measurements were carried out utilizing the UAM setup. Following the designation of the thermal conductivity data, the filled stars symbols correspond to the experiments taken at specially designed setups, the open symbols to those in a commercial device. As for the colors, like throughout the paper, red color accounts for ceramics sintered at 1600 °C and blue for the ones sintered at 1000 °C. Results are presented in Figure 6.

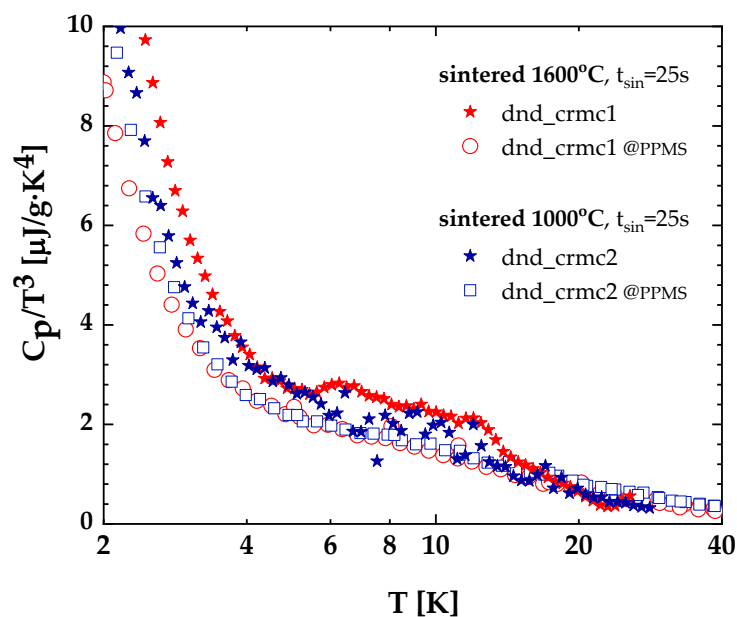


Figure 7. Low temperature specific heat displayed as C_p/T^3 : T of detonated nanodiamond ceramics sintered at different temperatures.

Looking at the low temperature behavior, one can still not distinguish between the experimental data of particular ceramic samples down to about 4 K. Furthermore, as the temperature dependence is almost the same below, it could be stated that the sintering temperature does not appear to have any influence on the low-temperature-specific heat. However, there is a small but clear difference in absolute values obtained on particular devices. One of the reasons behind this might be the individual systematic errors of the calorimeters, the other stemming from the particular sample pieces used during the experiments. In the case of the commercial setup, the sample size was limited by the measuring table dimensions and needed to be cut out of the cylindrical ceramic, and the UAM calorimeter allowed the use of the whole sample, which could result in different contributions of the defective regions in the bulk piece of the ceramic. Given the C_p/T as a function of T^2 representation (Figure 6), one clearly confirms the presence of a linear term in $C_p(T)$. The obtained coefficients of $\sim 20 \times 10^{-6} \text{ J/gK}^2$ are one order of magnitude larger than the typical values of a linear term found in glasses due to TLS, although they are comparable to those found in some disordered crystals [42]. Therefore, its origin may well be the same as in the latter. From the slope of the fit, the Debye temperature was calculated to be 482 K (± 6 K) for both samples. The obtained value of θ_D is high, close to the nanodiamond thin films by Wang et al. [43], but certainly below the one of crystalline bulk diamond [44].

An unexpected, a very pronounced upturn in the specific heat with lowering the temperatures is present in both samples, most likely reminiscent of a low-T Schottky anomaly attributable to some impurity inherent to the fabrication process. Those Schottky-like contributions could also affect the slight discrepancies between absolute specific heat values obtained for the corresponding ceramic samples in different calorimetric setups (entire sample for UAM calorimetric device, a piece for PPMS system).

In Figure 7 the specific heat is represented as C_p/T^3 vs. T , so that the departure of the low-temperature data from the Debye behavior expected for crystalline materials is more clearly evidenced.

3.3. Thermal Diffusivity

One of the parameters conditioning the possible application of a material is its ability to dissipate heat, known as thermal diffusivity α , which can be evaluated using the formula below:

$$\alpha = \frac{\kappa}{\rho \cdot C_p} \quad (1)$$

where κ stands for thermal conductivity at a given temperature; C_p is the specific heat at the same temperature; ρ is the density of the material. The density of the measured nanodiamond ceramics was determined, based on their geometrical dimensions and sample masses, to be $2.40 \pm 0.12 \text{ kg/m}^3$ and $2.49 \pm 0.13 \text{ kg/m}^3$ for the **dnd_crmc1** (sintered at $1600 \text{ }^\circ\text{C}$) and **dnd_crmc2** (sintered at $1000 \text{ }^\circ\text{C}$), respectively. Although the approximation is rough, similar ρ values are found in the literature [41,45]. The calculations were performed based on the thermal conductivity and heat capacity measurements carried out on the same samples in the PPMS setup, as it included the whole temperature range of interest. The results are presented in Figure 8.

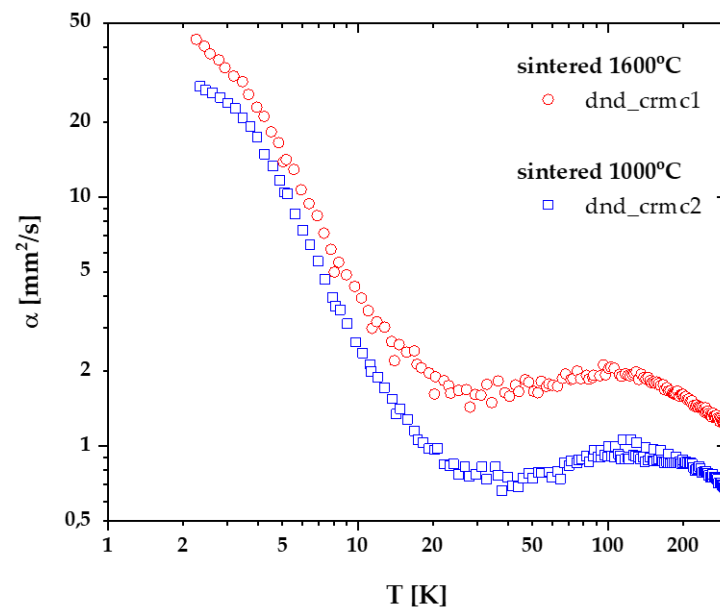


Figure 8. Thermal diffusivity of detonated nanodiamond ceramics sintered in different temperatures.

The temperature dependence of thermal diffusivity for both ceramic samples of detonated nanodiamonds exhibits a relatively similar behavior shifted slightly along the Y axis. With higher sintering temperature, one observes a slight increase in thermal diffusivity. Starting from the lowest investigated temperatures thermal diffusivity drops by an order of magnitude up to 25 K, then stabilizes finally with a further temperature increase one can observe a smeared thermal diffusivity hump with a maximum around 120 K. At room temperature the thermal diffusivity values are $1.22 \text{ mm}^2/\text{s}$ for the ceramic sintered at $1600 \text{ }^\circ\text{C}$ and half the value for the one sintered at $1000 \text{ }^\circ\text{C}$. Such low values of thermal diffusivity parameter are mostly caused by the ceramic microstructure and the high thermal resistance at grain boundaries, which was previously shown in thermal conductivity results.

3.4. Phonon Mean Free Path

In order to bring the nature of main phonon scattering mechanisms closer, one can estimate the phonon mean free path l_{ph} based on the simple kinetic gas equation:

$$\kappa(T) = 1/3 \cdot C_p(T) \cdot v \cdot l_{ph}(T) \quad (2)$$

where $\kappa(T)$ is the thermal conductivity, $C_p(T)$ stands for the specific heat and v is the sound velocity, which was assumed to be 13,430 m/s from ref. [40]. The results of the calculations are presented in Figure 9.

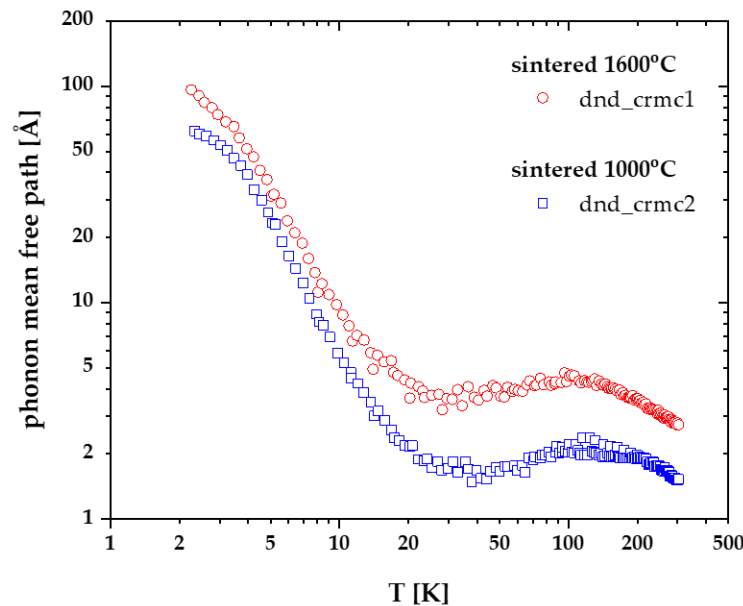


Figure 9. Phonon mean free path in differently sintered nanodiamond ceramics as a function of temperature.

For the calculations of the phonon mean free path the results of temperature-dependent thermal conductivity coefficient and heat capacity measured with PPMS setup were again used. The phonon mean free path relation of particular detonated nanodiamond ceramics looks very much like the thermal diffusivity parameter, which is a natural consequence of the similarity of Equations (1) and (2) used for the estimation of particular properties. The shape of individual curves shows much resemblance with the phonon mean free path data of diamond films presented in [40] but with somewhat lower absolute values. The obtained results once again prove the earlier conclusions. The strongly hindered heat flow in the investigated materials is confirmed by the relatively small values of the phonon mean free path. One can also notice a slight change of slope in the phonon mean free path temperature relation below 4 K, which was inherited from the Schottky anomaly in specific heat.

4. Conclusions

Thermal properties of detonated nanodiamond ceramics sintered in different conditions were studied both in specially designed setups and commercial devices. The resulting temperature dependence of thermal conductivity is dominated by the polycrystalline character of the ceramics in the whole investigated temperature range. At room temperature, increasing the sintering temperature from 1000 °C to 1600 °C induces an enhancement of heat flow by a factor of 1.5. On the other hand, reducing the sintering time from 25 s to 11 s, for the ceramics sintered at 1000 °C, causes a drop in thermal conductivity value by half. Low-temperature behavior indicates a strong influence of grain boundaries phonon scattering processes. Specific heat data do not exhibit the previous large sensitivity to the sample preparation. Only at the lowest temperatures an unexpected upturn in C_p/T vs. T^2 is evidenced reminiscent of the Schottky anomaly, inherited probably from the fabrication process. The linear contribution to the specific heat is also present with a value of approx. 20 $\mu\text{J/gK}$ and the calculated Debye temperature is 482 ± 6 K. The departure from the classical Debye behavior is clearly evidenced.

Supplementary Materials: The following Supporting Information can be downloaded at: <https://www.mdpi.com/article/10.3390/cryst12121774/s1>, Figure S1: XRD patterns of the detonated nanodiamond ceramic samples: top—ceramic sintered at 1000 °C and bottom—ceramic sintered at 1600 °C.

Author Contributions: D.S. and M.A.R.: writing—review and editing, formal analysis; D.S.: data curation, writing—original draft preparation, investigation; M.A.R.: supervision. All authors have read and agreed to the published version of the manuscript.

Funding: The current post-doc stay of D.S. is funded by the Bekker Programme of the Polish National Agency of Academic Exchange (Grant number BPN/BEK/2021/1/00091). M.A.R. acknowledges financial support by the Ministerio de Ciencia e Innovación of Spain (Grant PID2021-127498NB-I00/AEI/FEDER/10.13039/501100011033), as well as from the Autonomous Community of Madrid through program S2018/NMT-4321 (NANOMAGCOST-CM).

Data Availability Statement: The data presented in this study are available from corresponding author on request.

Acknowledgments: The low temperature heat capacity studies were performed at the UAM during the Short Term Scientific Mission funded by CA16218—Nanoscale coherent hybrid devices for superconducting quantum technologies (NANOCOBYBRI) European Cooperation in Science and Technology COST. The authors are grateful to Manuel Moratalla for his assistance in those experiments. The authors would like to thank Halina Misiorek for providing the detonated nanodiamond ceramic samples.

Conflicts of Interest: The authors declare no conflict of interest.

References

1. Dolmatov, V. Chapter 21: Detonation Nanodiamonds Section IV: Nanodiamonds. In *Carbon Nanomaterials Sourcebook: Graphene, Fullerenes, Nanotubes and Nanodiamonds*; CRC Press: Boca Raton, FL, USA, 2016. [CrossRef]
2. Vul', A.; Dideikin, A.; Aleksenskii, A.; Baidakova, M.V. Chapter 2: Detonation Nanodiamonds: Synthesis, Properties and Applications. In *Nanodiamond*; RSC Nanoscience and Nanotechnology: Cambridge, UK, 2014. [CrossRef]
3. Greiner, N.R.; Phillips, D.S.; Johnson, J.D.; Volk, F. Diamonds in detonation soot. *Nature* **1988**, *333*, 440. [CrossRef]
4. Gruen, D.M.; Shenderova, O.A.; Vul', A. Section III—Detonation nanodiamond. In *Synthesis, Properties and Applications of Ultrananocrystalline Diamond*; Springer: Berlin/Heidelberg, Germany, 2009. [CrossRef]
5. Zhang, Y.; Rhee, K.; Hui, D.; Park, S.-J. A critical review of nanodiamond based nanocomposites: Synthesis, properties and applications. *Compos. Part B Eng.* **2018**, *143*, 19. [CrossRef]
6. Baidakova, M.; Vul', A. New prospects and frontiers of nanodiamond clusters. *J. Phys. D Appl. Phys.* **2007**, *40*, 6300. [CrossRef]
7. Krueger, A. New Carbon Materials: Biological Applications of Functionalized Nanodiamond Materials. *Chem. A Eur. J.* **2008**, *14*, 1382. [CrossRef] [PubMed]
8. Dolmatov, V.; Ozerin, A.; Kulakova, I.; Bochechka, O.; Lapchuk, N.; Myllymäki, V.; Vehanen, A. Detonation nanodiamonds: New aspects in the theory and practice of synthesis, properties and applications. *Russ. Chem. Rev.* **2020**, *89*, 1428. [CrossRef]
9. Mochalin, V.; Shenderova, O.; Ho, D.; Gogotsi, Y. The properties and applications of nanodiamonds. *Nat. Nanotechnol.* **2011**, *7*, 11. [CrossRef]
10. Danilenko, V. Nanodiamonds: Problems and prospects. *J. Superhard Mater.* **2010**, *32*, 301. [CrossRef]
11. Schrand, A.; Ciftan-Hens, S.; Shenderova, O. Nanodiamond Particles: Properties and Perspectives for Bioapplications. *Crit. Rev. Solid State Mater. Sci.* **2009**, *34*, 18. [CrossRef]
12. Dolmatov, V. Detonation-synthesis nanodiamonds: Synthesis, structure, properties and applications. *Russ. Chem. Rev.* **2007**, *76*, 339. [CrossRef]
13. Caccia, M.; Rodríguez, A.; Narciso, J. Diamond Surface Modification to Enhance Interfacial Thermal Conductivity in Al/Diamond Composites. *J. Miner. Met. Mater. Soc.* **2014**, *66*, 920. [CrossRef]
14. Zhang, F.; Fan, K.; Saba, F.; Yu, J. Graphene reinforced-graphitized nanodiamonds matrix composites: Fabrication, microstructure, mechanical properties, thermal and electrical conductivity. *Carbon* **2020**, *169*, 416. [CrossRef]
15. Chen, G. Non-Fourier phonon heat conduction at the microscale and nanoscale. *Nat. Rev. Phys.* **2021**, *3*, 555. [CrossRef]
16. Hoogeboom-Pot, K.; Hernandez-Charpak, J.; Gu, X.; Frazer, T.; Anderson, E.; Chao, W.; Falcone, R.; Yang, R.; Murnane, M.; Kapteyn, H.; et al. A new regime of nanoscale thermal transport: Collective diffusion increases dissipation efficiency. *Proc. Natl. Acad. Sci. USA* **2015**, *112*, 4846. [CrossRef]
17. Balandin, A.; Wang, K. Significant decrease of the lattice thermal conductivity due to phonon confinement in a free-standing semiconductor quantum well. *Phys. Rev. B* **1998**, *58*, 1544. [CrossRef]
18. Bochicchio, I.; Giannetti, F.; Sellitto, A. Heat transfer at nanoscale and boundary conditions. *Z. Für Angew. Math. Und Phys.* **2022**, *73*, 147. [CrossRef]

19. Bao, H.; Chen, J.; Gu, X.; Cao, B. A Review of Simulation Methods in Micro/Nanoscale Heat Conduction. *ES Energy Environ.* **2018**, *1*, 16. [CrossRef]
20. Kidalov, S.; Shakhov, F.; Vul, A. Thermal conductivity of sintered nanodiamonds and microdiamonds. *Diam. Relat. Mater.* **2008**, *17*, 844. [CrossRef]
21. Vlasov, A.; Ralchenko, V.; Gordeev, S.; Zakharov, D.; Vlasov, I.; Karabutov, A.; Belobrov, P. Thermal properties of diamond/carbon composites. *Diam. Relat. Mater.* **2000**, *9*, 1104. [CrossRef]
22. Su, S.; Wang, J.; Wei, J.; Qiu, J.; Wang, S. Thermal conductivity studies of electrophoretically deposited nanodiamond arrays. *Mater. Sci. Eng. B* **2017**, *225*, 54. [CrossRef]
23. Vasiliev, O.; Muratov, V.; Kulikov, L.; Garbuz, V.; Duda, T. Special features of the heat capacity of detonation nanocrystalline diamond. *J. Superhard Mater.* **2015**, *37*, 388. [CrossRef]
24. Tritt, T. *Thermal Conductivity Theory, Properties, and Applications*; Springer: Berlin/Heidelberg, Germany, 2003. [CrossRef]
25. Pobell, F. *Matter and Methods at Low Temperatures*; Springer: Berlin/Heidelberg, Germany, 2007. [CrossRef]
26. Aleksenskiy, A.; Eydelman, E.; Vul', A. Deagglomeration of Detonation Nanodiamonds. *Nanosci. Nanotechnol. Lett.* **2011**, *3*, 68. [CrossRef]
27. Krüger, A.; Kataoka, F.; Ozawa, M.; Fujino, T.; Suzuki, Y.; Aleksenskii, A.; Vul', A.; Ōsawa, E. Unusually tight aggregation in detonation nanodiamond: Identification and disintegration. *Carbon* **2015**, *43*, 1722. [CrossRef]
28. Szewczyk, D.; Jeżowski, A.; Krivchikov, A.I.; Tamarit, J.L. Influence of thermal treatment on thermal properties of adamantane derivatives. *Low Temp. Phys.* **2015**, *41*, 469. [CrossRef]
29. Quantum Design, Physical Property Measurement System. Thermal Transport Option User's Manual. 2002. Available online: https://www.mrl.ucsb.edu/sites/default/files/mrl_docs/instruments/PPMSTTOmanualB0.pdf (accessed on 1 December 2022).
30. Maldonado, O. Pulse method for simultaneous measurement of electric thermopower and heat conductivity at low temperatures. *Cryogenics* **1992**, *32*, 908. [CrossRef]
31. Perez-Enciso, E.; Ramos, M.A. Low-temperature calorimetry on molecular glasses and crystals. *Thermochim. Acta* **2007**, *461*, 50. [CrossRef]
32. Pérez-Castañeda, T.; Azpeitia, J.; Hanco, J.; Fente, A.; Suderow, H.; Ramos, M.A. Low-Temperature Specific Heat of Graphite and CeSb₂: Validation of a Quasi-adiabatic Continuous Method. *J. Low Temp. Phys.* **2013**, *173*, 4. [CrossRef]
33. Hwang, J.; Lin, K.; Tien, C. Measurement of heat capacity by fitting the whole temperature response of a heat-pulse calorimeter. *Rev. Sci. Instrum.* **1997**, *68*, 94. [CrossRef]
34. Quantum Design, Physical Property Measurement System. Heat Capacity Option User's Manual. 2004. Available online: https://www.mrl.ucsb.edu/sites/default/files/mrl_docs/instruments/hcapPPMS.pdf (accessed on 1 December 2022).
35. Rudajevová, A.; Švantner, M.; Vasylyev, D.; Musil, O.; Lang, V. Influence of Radiation Losses on Thermal Conductivity Determination at Low Temperatures. *Int. J. Thermophys.* **2006**, *27*, 1241. [CrossRef]
36. Kidalov, S.; Shakhov, F.; Vul', A.; Ozerin, A. Grain-boundary heat conductance in nanodiamond composites. *Diam. Relat. Mater.* **2010**, *19*, 976. [CrossRef]
37. Shakhov, F.; Meilakhs, A.; Eidelman, E. Changes in the mechanism of heat transfer in passing from microparticles to nanoparticles. *Tech. Phys. Lett.* **2016**, *42*, 252. [CrossRef]
38. Barman, S.; Srivastava, G.P. Temperature dependence of the thermal conductivity of different forms of diamond. *J. Appl. Phys.* **2007**, *101*, 123507. [CrossRef]
39. Cahill, D.G.; Watson, S.K.; Pohl, R.O. Lower limit to the thermal conductivity of disordered crystals. *Phys. Rev. B* **1992**, *46*, 6131. [CrossRef]
40. Efimov, V.; Mezhev-Deglin, L. Phonon scattering in diamond films. *Phys. B Condens. Matter* **1999**, *263*, 745. [CrossRef]
41. Kidalov, S.; Shakhov, F.; Vul', A. Thermal conductivity of nanocomposites based on diamonds and nanodiamonds. *Diam. Relat. Mater.* **2007**, *16*, 2063. [CrossRef]
42. Ramos, M.A. Chapter 2: Low-Temperature Specific Heat of Glasses and Disordered Crystals. In *Low-Temperature Thermal and Vibrational Properties of Disordered Solids*; World Scientific Publishing Europe Ltd.: London, UK, 2022. [CrossRef]
43. Wang, Y.; Zhao, Q.; Zhao, Z.; Yin, Z.; Yang, Q.; Li, H. The Debye characteristic temperature of nanodiamond thin films. In Proceedings of the SPIE 7381, International Symposium on Photoelectronic Detection and Imaging 2009: Material and Device Technology for Sensors, 73810R, Beijing, China, 24 August 2009. [CrossRef]
44. Pässler, R. Efficient Debye Function Interpolation Formulae: Sample Applications to Diamond. *Recent Prog. Mater.* **2021**, *3*, 42. [CrossRef]
45. Vityaz, P.A.; Senyut, V.T. Compaction of Nanodiamonds Produced under Detonation Conditions and Properties of Composite and Polycrystalline Materials Made on Their Basis. *Phys. Solid State* **2004**, *46*, 764. [CrossRef]